Optica Applicata, Vol. X, No. 4, 1980

Numerical reconstruction of intensity distribution in the incoherent imaging*

I. Diffraction-limited systems

RENATA NOWAK, IRENEUSZ WILK

Institute of Physics, Technical University of Wrocław, Wrocław, Poland.

The numerical properties of the direct recovery method are discussed from the viewpoint of their importance in the problem of the image intensity reconstruction from the discrete and finite set of measurement results obtained by a square-law sampling system. The effect of many factors like: number of sampling points, value of sampling step, sizes of the integrating element and the like, on the numerical aspects of the procedure considered is examined. Both one- and two-dimensional cases are analyzed. It has been shown that the direct recovery method is very sensitive to even very small changes in the intensity spread function.

Introduction

In the most considered reconstruction procedures it is assumed that the amplitude or intensity distribution is known within the whole region of the image or in its chosen part (see [1, 2], for example).

Under typical experimental conditions this assumption is not fulfilled and the image is represented by a finite number of measurement results that depend on the measurement system and the configuration of measurement points.

This situation was discussed in the works [3-6], where a method of image intensity distribution from the discrete and finite set of the measurement results was proposed. This method was called the direct recovery method to emphasize its direct connection with the measurement results. Since the results obtained from the measurement performed by locating consecutively the measuring system with a square law detector at the respective points of the image plane are not identical with the image intensity distributions, the basic task of the reconstruction procedure is to recover the latters.

In this paper we will discuss some properties of the direct recovery method which are important for numerical examinations.

Direct recovery of the image intensity distribution for the incoherent imaging

For the sake of convenience we will remind in this section some ideas and notations used earlier in the works [3, 4]. Let the unknown incoherent object intensity distribution $I_{ob}(\alpha, \beta)$ placed at the plane P_I (fig. 1) be

* This work was carried out under the Research Project M.R. I.5.

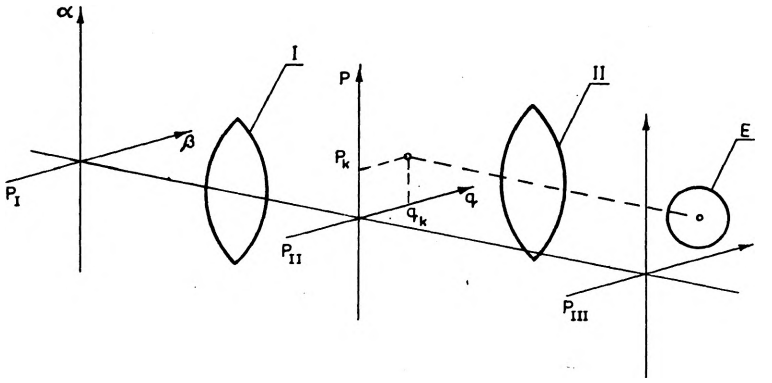

Fig. 1. Schemes of the imaging (I) and measuring (II) systems, respectively

imaged onto the plane P_{II} by the optical system I producing the image $I_{im}(p, q)$.

In the image plane N measurements of the image intensity distribution are performed by the measuring system II located consecutively at the respective N points of this plane.

Assume that the measuring system consists of the optical part imaging the object intensity distribution $I_{im}(p, q)$ onto the plane II and of an integrating element (square-law-detector) located in this plane, which transduces the whole incident light energy into a signal of different nature (an electric signal, for instance). In the simplest case the measuring system II may be reduced to the integrating element alone placed immediately in the image plane P_{II}.

As it is well known the operation of a linear stationary optical system with incoherent illuminator may be described by an integral operator associating the object intensity distribution $I_{ob}(\alpha, \beta)$ with the image intensity distribution $I_{im}(p, q)$ by the formula

$$I_{im}(p, q) = \int I_{ob}(\alpha, \beta)\varphi^{I}(p-\alpha, q-\beta)\,d\alpha d\beta. \tag{1}$$

The kernel of this integral transformation is the incoherent point spread function for the magnification of the imaging system normalized to unity.

Analogically, the imaging by the optical part of the measuring system may be described as

$$I(u, v) = \int I_{im}(p, q)\varphi^{II}[u-(p-p_k), v-(q-q_k)]\,dp dq, \tag{2}$$

where $\varphi^{II}[u-(p-p_k), v-(q-q_k)]$ denotes the incoherent point spread function for the imaging system II positioned at the point (p_k, q_k); the magnification of this system being also normalized to unity.

In order to determine the correlation between the measurement result and the real intensity distribution in the image $I_{im}(p, q)$ it suffices to

notice that the functional [7]:

$$\Phi(p-p_k, q-q_k) \stackrel{\text{df}}{=} \int_E \varphi^{\text{II}}[u-(p-p_k), v-(q-q_k)]\,du\,dv \tag{3}$$

informs by definition what part of energy coming from any image point (p, q) reaches the integrating element at the position (p_k, q_k) of the measuring system.

If the measurement result at the image point is understood as the value of the energy reaching the integrating element (p_k, q_k) then the measurement may be written in the form of an integral transform of the object distribution $I_{\text{ob}}(p, q)$ [4], i.e.

$$y(p_k, q_k) = \int_E I(u, v)\,du\,dv = \int I_{\text{im}}(p, q)\,\Phi(p-p_k, q-q_k)\,dp\,dq. \tag{4}$$

By assuming that an unknown object consists of an array of finite number of lighting points

$$I_{\text{ob}}(\alpha, \beta) = \sum_{i=1}^{N} C_i\,\delta(\alpha-\alpha_i)\,\delta(\beta-\beta_i) \tag{5}$$

and substituting this expression to the eq. (1) and next the resulting expression to (4) the dependence relating the measurement results with the quantities characterizing the imaging and measuring systems is obtained

$$y(p_k, q_k) = \sum_{i=1}^{N} \int C_i\varphi^{\text{I}}(p-\alpha_i, q-\beta_i) \times \Phi(p-p_k, q-q_k)dp\,dq, \tag{6}$$

or shortly

$$y(p_k, q_k) = \sum_{i=1}^{N} C_i R_{ik},\ k = 1, \ldots, N, \tag{7}$$

where the matrix

$$\{R_{i,k}\} = \left\{\int \varphi^{\text{I}}(p-\alpha_i, q-\beta_i)\,\Phi(p-p_k, q-q_k)\ dp\ dq\right\} \tag{8}$$

called the reconstruction matrix [4] has the elements defined completely by the properties of the imaging system I and measuring system II.

The order of this matrix is defined by the number of sampling (measuring) points $k = 1, \ldots, N$.

The solution of the system of linear eqs. (7) with respect to the unknown weighting coefficient C_i allows to reconstruct the real intensity at the discrete points of the image [4] as:

$$I(p_k\,q_k) = \sum_{i=1}^{N} C_i\varphi^{\text{I}}(\alpha_i-p_k, \beta_i-q_k). \tag{9}$$

It is evident that this solution is unique if and only if we know that the object has exactly the structure assumed in (5), i.e. if we know exactly the positions of the lighting points. It is usually not the case. In the general

case in order to find the extreme (maximal and minimal) possible a posteriori image intensity distributions still consistent with the same set of measurement results $y(p_k, q_k)$ let us first assume that the subsequent positions of the measuring system II coincide with the local maxima of the intensity distribution to be recovered. Let us additionally assume that the recovered intensity distribution is generated by an object of the form (5) with suitably positioned lighting points (fig. 2a). Under such an assumption the respective reconstruction matrix will be called the upper bound recon-

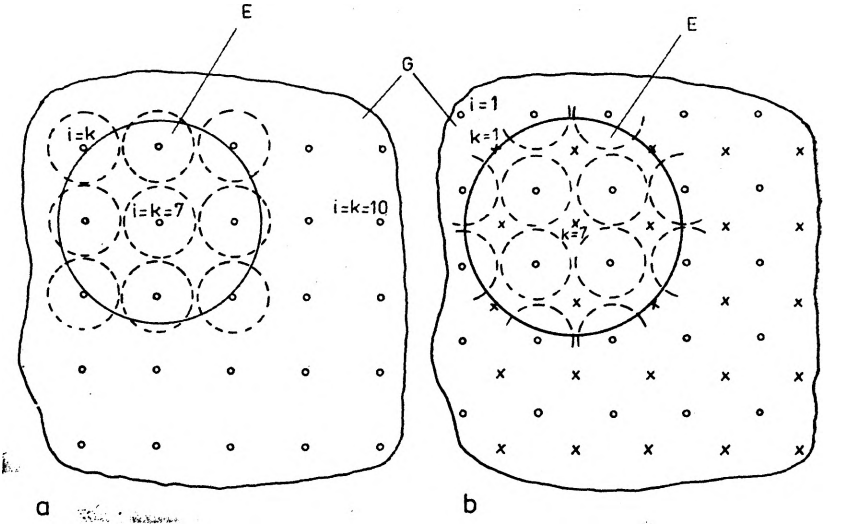

Fig. 2. The mutual configuration of the sampling points (×) and imaged points (○) in the case of:
a. upper bound reconstruction (the sampling points coincide with the imaged points), b. lower bound reconstruction (the sampling points lie between the imaged points)

struction matrix $R_{i,k}^{\max}$ [4]. The corresponding image intensity distribution estimated from eq. (1) will assume the possible values of the light intensity at the sampling point (p_k, q_k) 4, i.e.

$$I^{\max}(p_k, q_k) = \sum_{i=1}^{N} C_i^{\max} \varphi(\alpha_i - p_k, \beta_i - q_k). \tag{10}$$

When considering an opposite situation, i.e. when assuming that the same positions (p_k, q_k) of the measuring system coincide with the local minima of the sought image intensity distribution (fig. 2b) (again assumed to be generated by the suitably positioned object of the form (5)) also consistent with the same measurement results, we obtain the other extreme (minimal) intensity distribution by using the same recovery procedure. The matrix of this recovery procedure will be called the lower bound reconstruction matrix $R_{i,k}^{\min}$ and the reconstructed image intensity distribution at the points (p_k, q_k) given by

$$I^{\min}(p_k, q_k) = \sum_{i=1}^{N} C_i^{\min} \varphi(\alpha_i' - p_k, \beta_i' - q_k) \tag{11}$$

will be respectively the lower bound image intensity distribution. From eqs. (10) and (11) it is evident that by applying the above recovery procedure we may obtain many solutions, i.e. many image intensity distributions at the sampling points which would be contained between the above extreme cases represented by $I^{\max}(p_k, q_k)$ and $I^{\min}(p_k, q_k)$.

The knowledge of the extreme values of the image intensity allows to determine in a natural way the reconstruction (measurement) error defined as

$$\Delta I = \frac{1}{2} \left| I^{\max}(p_k, q_k) - I^{\min}(p_k, q_k) \right| \tag{12}$$

at each sampling points (p_k, q_k), as well as the average reconstructed image intensity distribution defined as

$$\langle I \rangle = \frac{1}{2} \left| I^{\max}(p_k, p_k) + I^{min}(p_k, q_k) \right|. \tag{13}$$

The method and the algorithms useful in numerical calculations of the matrix elements $R_{k,i}$ for the aberration-free optical systems of rotational symmetry have been presented in [6] under the assumption that the imaging and measuring systems are space-invariant.

Numerical properties of the direct recovery method

In this section we will discuss some numerical properties of the direct recovery procedure important from the practical viewpoint. In particular, we shall examine the effect of such factors like: the number of sampling points, the step of sampling, the size of the integrating element and the like, on the construction procedure. Both the one-dimensional and two-dimensional cases are analysed.

Calculations were performed for the diffraction-limited system of f-number 4.5 under assumption that the object was located at infinity.

The measuring system was reduced to a circular integrating element of $R_E = 0.0016$ mm radius, while the wavelength of the incident light beam was $\lambda = 0.00058$ mm. As it will be shown later the reduction of the measuring system to a uniform integrating element only has no essential influence on the reconstruction results for the diffraction-limited systems.

The distance between the sampling (measuring) points in the image intensity distribution was assumed to be equal to the Rayleigh resolution distance.

For the one-dimensional objects the reconstruction procedure has been examined for $k = 2, \ldots, 5$, and $k = 10$ sampling points (table 1), while for two-dimensional objects the respective numbers of the sampling points were $k = 4, 9, 25$, and 49 (table 3). For numerical purposes we have postulated the measurement results $y(p_k, q_k)$ at the sampling points to be equal to unity, except for the boundary sampling points (tables 1

Table 1

Postulated distribution of the sampling results for one-dimensional object for different numbers of the sampling points

Number of sampling points	Postulated distribution of the intensity measurement results									
2	1	0.5								
3	1	1	0.5							
4	1	1	1	0.5						
5	1	1	1	1	0.5					
10	1	1	1	1	1	1	1	1	1	0.5

Table 2

The influence of the number of sampling points on the reconstruction of the intensity distribution in the one-dimensional objects

Number of sampling points	Reconstructed upper bound image intensity distribution I^{max}				
2	0.188	0.086			
3	0.184	1.187	0.087		
4	0.185	0.173	0.179	0.087	
5	0.185	0,174	0.174	0.179	0.087
10	0.185	0.174	0.175	0.175	0.175
	0.175	0.175	0.175	0.178	0.087
Number of sampling points	Reconstructed lower bound image intensity distribution I^{min}				
2	0.136	0.066			
3	0.136	0.136	0.068		
4	0.136	0.134	0.136	0.068	
5	0.136	0.137	0.137	0.138	0.068
10	0.137	0.137	0.137	0.137	0.137
	0.137	0.137	0.137	0.136	0.068

Table 3

The postulated intensity distribution in the two-dimensional objects depending on the number of sampling points. For the values underlined the reconstructed intensities are represented in table 4

Number of sampling points	Postulated distribution of intensity measurement results						
49	1	1	1	1	1	1	0.5
	1	1	1	1	1	1	0.5
	1	1	1	1	1	1	0.5
	1	1	1	1	1	1	0.5
	1	1	1	1	1	1	0.5
	1	1	1	1	1	1	0.5
	0.5	0.5	0.5	0.5	0.5	0.5	0.2
29	1	1	1	1	0.5		
	1	1	1	1	0.5		
	1	1	1	1	0.5		
	1	1	1	1	0.5		
	0.5	0.5	0.5	0.2	0.5		
9	1	1	0.5				
	1	1	0.5				
	0.5	0.5	0.2				
4	1	0.5					
	0.5	0.2					

and 3) for which the half-values were assumed. Such an assumption is connected with the accepted configurations of the sampling and imaged points, respectively (fig. 2). Hovewer, by comparing the situation of the integrating element, as positioned at the points $k = 7$, and $k = 10$, for instance, it may be seen that at the point $k = 7$, the result of measurement is influenced by the contributions coming from a greater number of neighbouring image points than e.g. $k = 10$. Thus, it may be expected that the result of recovered image intensity will be greater for $k = 7$ than for $k = 10$, since it is only one of many contributors to the respective measurement results. Of course, the postulated results of measurements (tables 1 and 3) are some of infinitely many possible free terms of the reconstruction eq. (7). It should be noticed that for physical reasons all the solutions of this equation fulfil the condition $C_i \geqslant 0$. This condition is fulfilled automatically, when the real measurements are performed, however, it may be violated when the measurement procedures are simulated. In the later case the

Table 4

The influence of the number of sampling points on the image intensity reconstruction for the two-dimensional objects. In this table the results for selected points from the table 3 are used

Number of sampling points	Reconstructed upper bound image intensity distribution I^{max}						
49	0.175	0.166	0.166	0.166	0.166	0.171	0.083
	0.083	0.080	0.080	0.080	0.080	0.082	0.030
25	0.178	0.169	0.170	0.174	0.185		
	0.085	0.082	0.082	0.084	0.031		
9	0.178	0.175	0.082				
	0.085	0.083	0.034				
4	0.185	0.085					
	0.085	0.027					
	Reconstructed lower bound image intensity distribution I^{min}						
49	0.071	0.073	0.073	0.073	0.073	0.071	0.032
	0.032	0.034	0,034	0.034	0.034	0.033	0.017
25	0.079	0.081	0.081	0.079	0.041		
	0.041	0.042	0.042	0.041	0.017		
9	0.078	0.079	0.040				
	0.040	0.041	0.017				
4	0.163	0.057					
	0.056	0.022					

appearance of the negative solutions signals the inproper assumption of the measurement results.

From the calculated examples it follows that the reconstructed image intensity distribution depends only weakly on the number of sampling points.

This property of the direct recovery is worth noting due to its practical importance. It eliminates the necessity of solving a great number of linear eq. (7) (in order to obtain the sufficient accuracy in the reconstruction process) which would have a disadvantageous influence on the numerical calculation accuracy.

Except for reconstruction reduced to two measuring points in the case of one-dimensional object (table 2) and for the reconstruction of four measuring points in the case of two-dimensional objects (table 4), the other examples of the calculated intensity distribution differ slightly from one another, in spite of the fact that the number of measuring and imaged points increases. In the case of the linear object recovery the changes of the reconstruction errors do not exceed 1% for $k > 2$, while for the

two-dimensional objects the reconstruction error stabilizes for $k > 4$. In the examples discussed the increase of the number of sampling points causes an increase of the reconstructed region. The opposite case, i.e. the increase in the sampling point number occurring within the same region, will be discussed in details in the next section.

The influence of the sampling step on the image intensity recovery

Similarly as in the previous cases, the calculations were performed for the imaging system of the f-number 4.5 and the integrating element of the circular shape and the radii $R_E = 0.0032$ mm and $R_E = 0.0016$ mm, respectively.

The discrete (punctual) image intensity distribution has been reconstructed in a two-dimensional region by using 25 sampling points located as indicated in fig. 2.

The changes of the reconstructed upper and lower bounds of image intensity distributions due to the increasing sampling step ($d = 0.0032$, 0.0038, 0.0064 mm) are illustrated in figs. 3-8. The subsequent numbers denote the sampling points, while the primed numbers denote the reduced upper bound intensity. The reconstructed upper and lower bound values of the intensity are mutually connected with some arrows. For instance, for the point 16 the result of sampling is assumed to be equal to 1 (table 3). As a result of reconstruction two values of the extreme admissible image intensity at this point are obtained (joined with an arrow in fig. 3). This should be understood so that all the possible values of real image intensity corresponding to the given sampling result lie within this interval.

From the figures 3, 4, and 5 it may be seen that with the increase of the sampling step the values of $\Delta I = \frac{1}{2}|I^{\max} - I^{\min}|$ increase, while the differences between the reconstructed average values of the image intensity are small for the middle points of the reconstructed region. By reducing the integrating element radius to its half-value (figs. 6-8) for the same sampling steps the observed diffraction effect of the reconstructed intensity distributions is much lower, in spite of the fact that the result of sampling in both the cases is the same. The greatest changes in the reconstruction error $\Delta I = \frac{1}{2}|I^{\max} - I^{\min}|$ are observed for the middle points, while the least ones occur at the edge points, i.e. for $k = 1, 5, 15, 20$, and so on (fig. 3). It turns out that the diversity of the reconstructed image intensity distributions depends on whether the energy contributions from the object points, reaching the integrating element at its given position, come from the central region (spread up to the first minimum) of respective spread function and called further the region I (of radius R_φ^{I}) or from its boundary regions only.

By comparing the estimates of the reconstruction errors ΔI given in table 5, for the integrating elements $R_E = 0.0032$ and $R_E = 0.0016$ mm

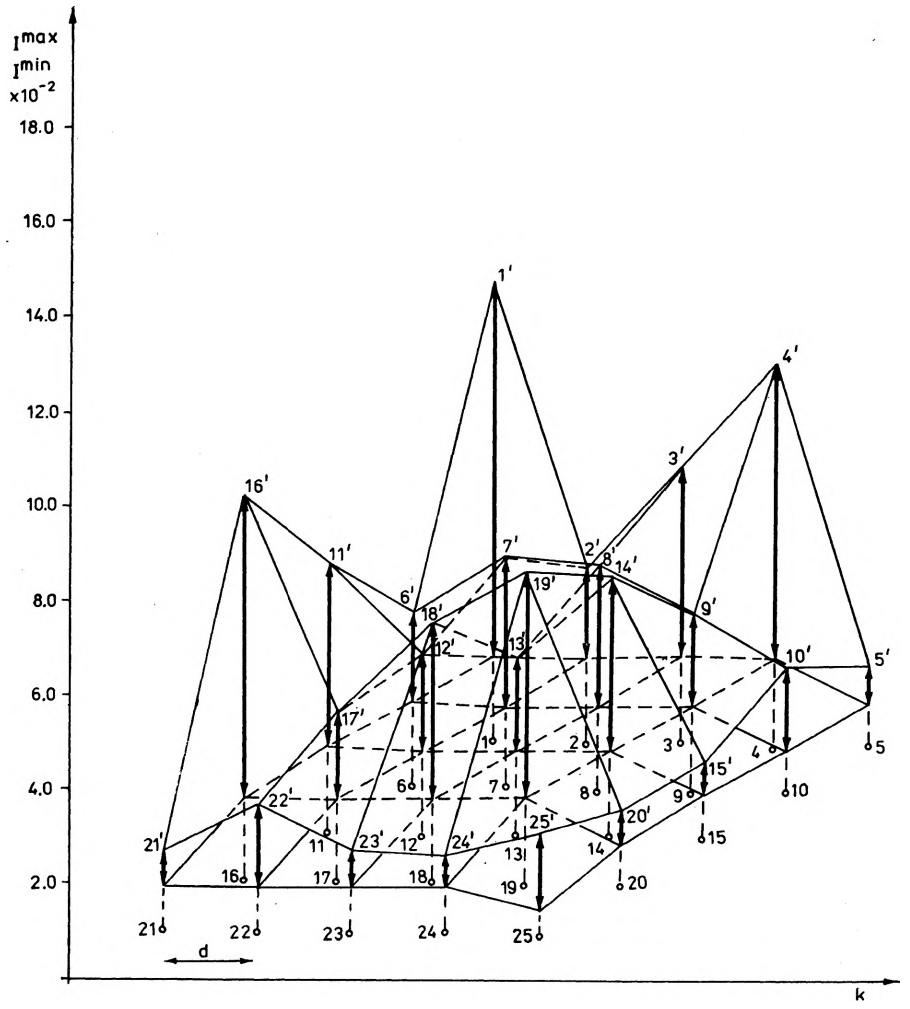

Fig. 3. The upper and lower reconstruction of the image intensity reconstruction. The f-number of the imaging system 4.5, the radius of the integrating element R_E = 0.0032 mm, the sampling step d = 0.0032 mm

and the same sampling steps $d = 0.0032$ it may be easily noticed that, despite the fact that the number of image points contributing to particular results in both reconstruction processes is approximately the same, the reconstructed image intensity distributions in the second case (fig. 7) are much less diversified than in the first one (fig. 4). Similarly, by comparing the results given in table 5 for $R = 0.0032$ mm and $d = 0.0064$ it may be seen that the reduction of both the sampling step and the integrating element radius by the factor 1/2 causes an essential increase of the number of image points taking an immediate part in the image intensity reconstruction procedure at the k-th sampling point, but it only slightly

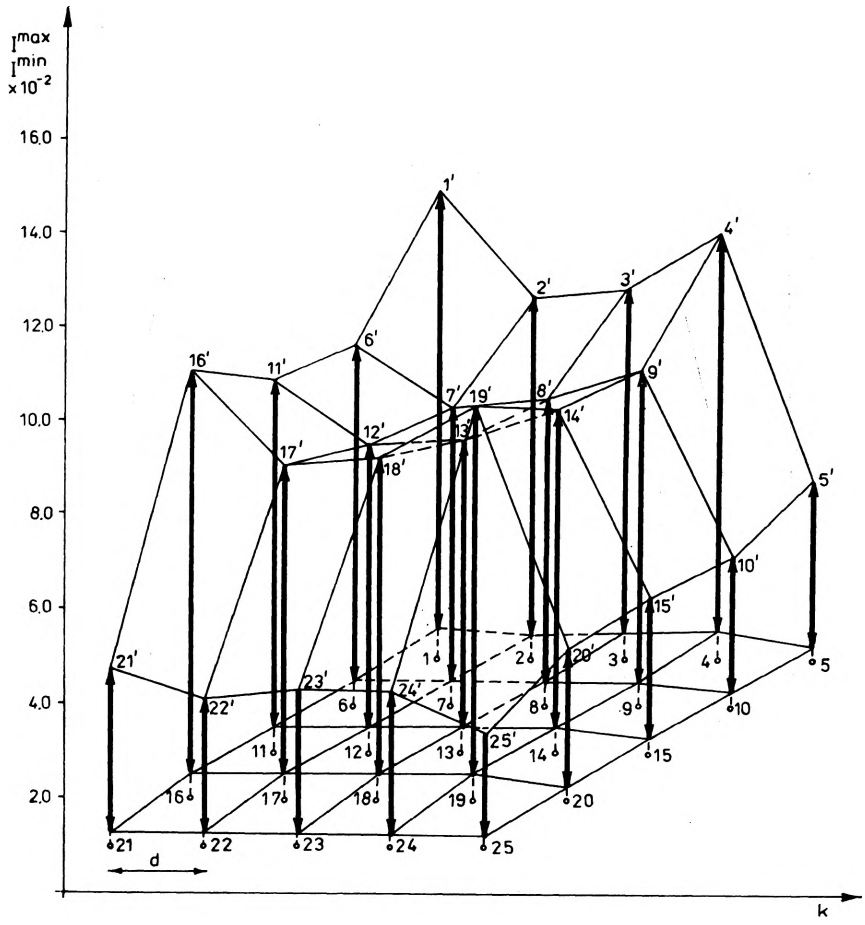

Fig. 4. The upper and lower bound reconstruction of the image intensity distribution. The *f*-number of the imaging system 4.5, the radius of the integrating element $R_E = 0.0032$ mm, the sampling step $d = 0.0038$ mm

affects the diversity of the reconstructed image intensity distributions corresponding to this situation (graphs in figs. 6 and 7). Thus the dominant effect on the reconstructed intensity distribution does not depend so much on the number of the image points taking immediate part in the reconstruction but on the fact that the energy contributions from these points come from the region limited by the first minimum of the spread function (as within this region the spread function changes most rapidly). This is explained in fig. 9 which illustrates the mutual positions of the integrating element and the spread functions associated with the positions of two closest image sampling points in the case of the image intensity reconstruction presented in figs. 3 and 5, and in figs. 6 and 8.

If the energy contributions from the closest neighbours come from the regions II of the respective spread functions, i.e. if the condition $d < R_E + R_\varphi^{II}$

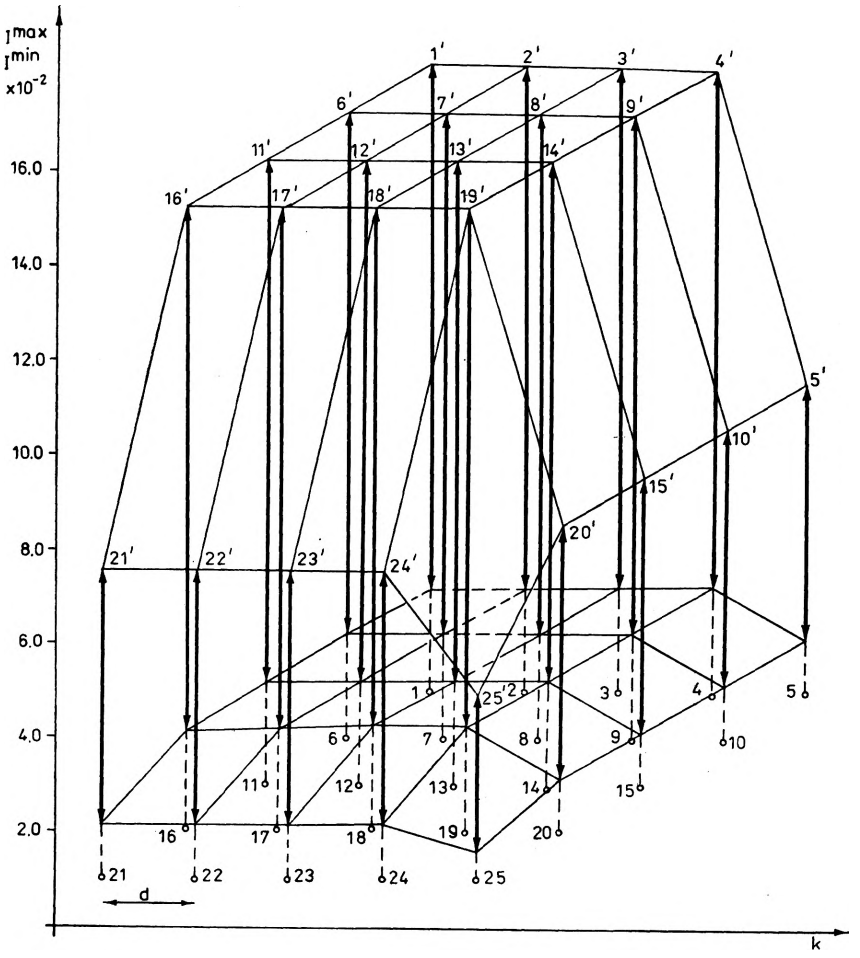

Fig. 5. The upper and lower bound reconstruction of the image intensity distribution. The f-number of the imaging system 4.5, the radius of the integrating element R_E = 0.0032 mm, the sampling step d = 0.0064 mm

is fulfilled (fig. 9ab and the graphs in fig. 3) then the reconstructed upper and lower bound intensity values are the more diversified the greater the energy contribution coming from the region I of the spread function. The degree of diversity of the reconstructed image intensity distributions lowers with the decrease of the energy contributions from the region I of the spread function. For the reasons discussed above the effect of differentiation of the reconstructed intensities for particular sampling points is much more distinct in the case of the upper bound reconstruction than in that of the lower bound reconstruction. When the energy contribution comes from the periphery regions of the spread function, i.e. when the condition $d \geqslant R_E + R_\varphi^{\mathrm{I}}$ (figs. 9cd) is fulfilled, the reconstructed

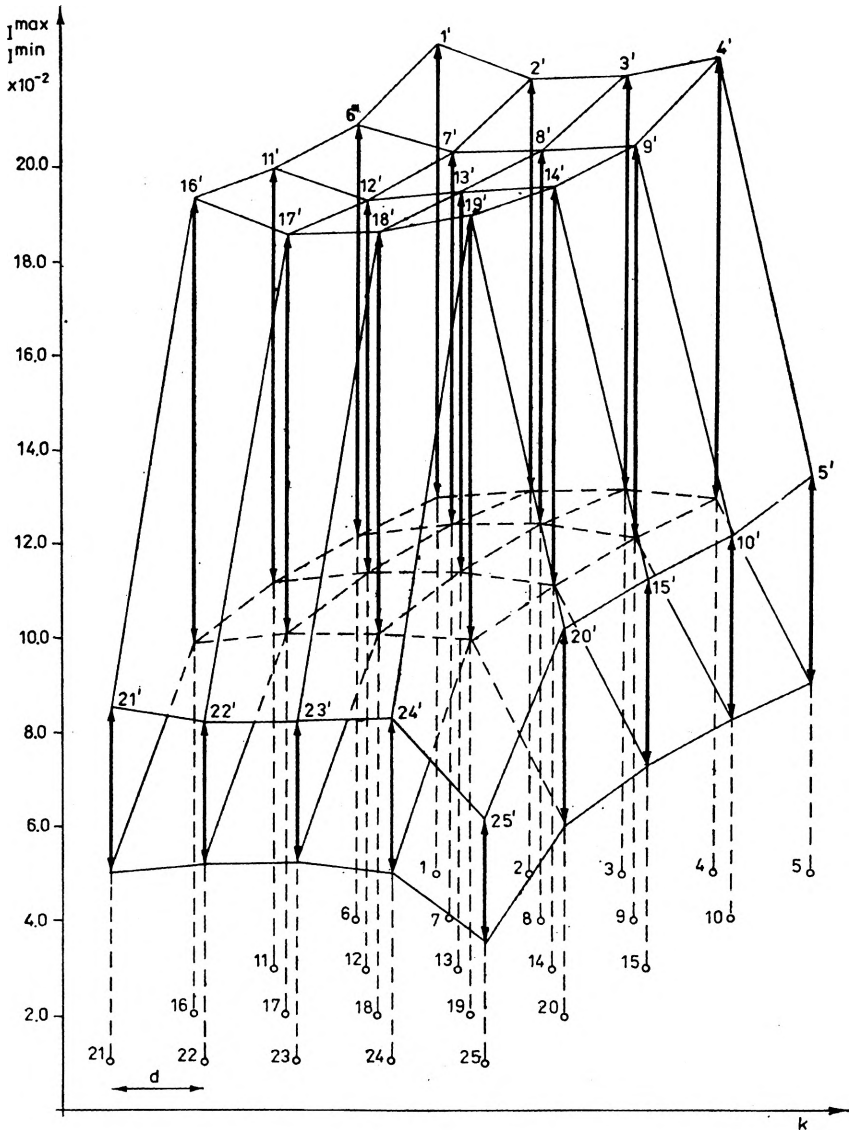

Fig. 6. The upper and lower bound reconstruction of the image intensity distribution. The f-number of the imaging system 4.5, the radius of the integrating element R_E = 0.0016 mm, the sampling step d = 0.0032 mm

values of intensity are the same for all the points (except for the marginal ones) or differ only slightly (fig. 5).

The example presented in fig. 8 requires a separate analysis. Here the effect of inversion of the extreme intensity distributions is observed. It appears namely that the reconstructed lower bound intensity distribution turns out to be greater than the respective reconstructed upper bound

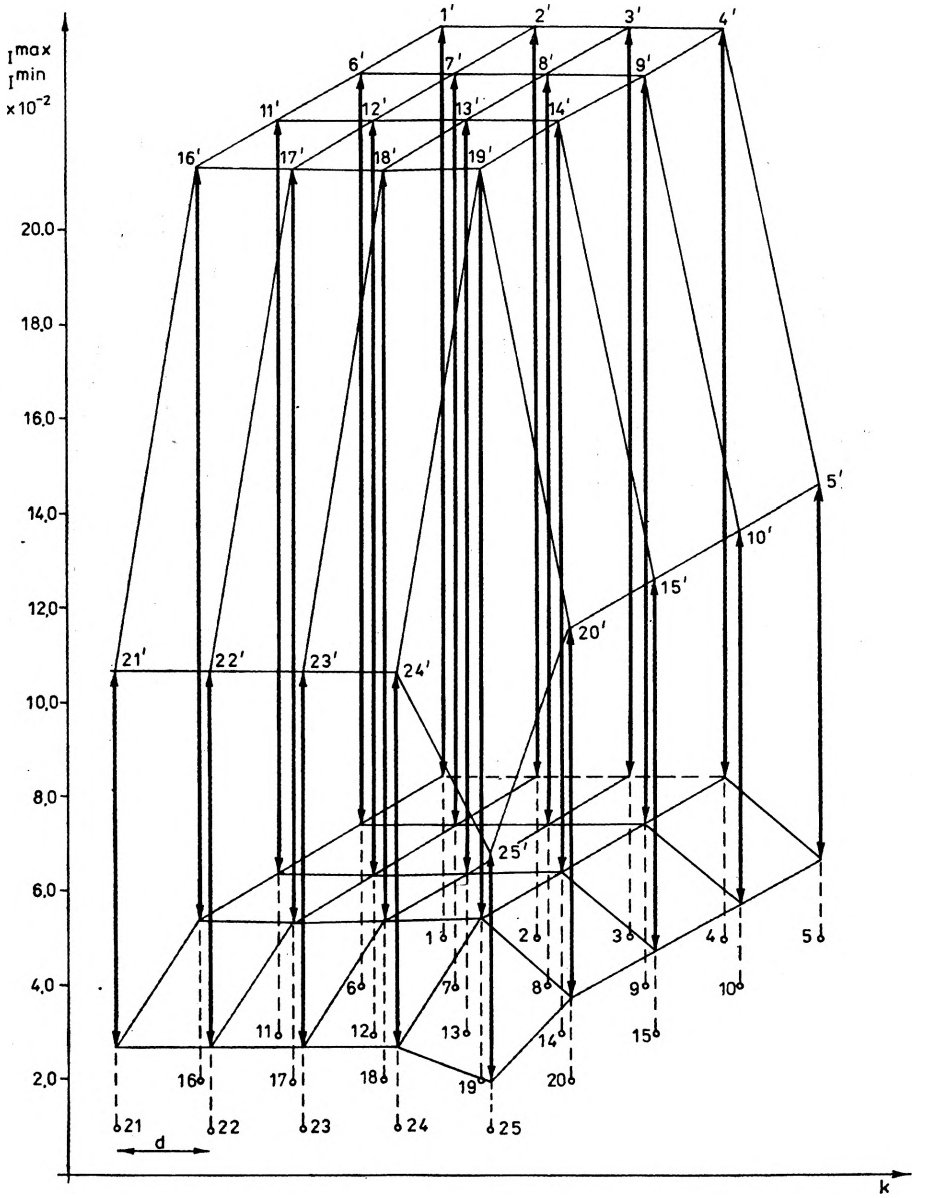

Fig. 7. The upper and lower bound reconstruction of the image intensity distribution. The f-number of the imaging system 4.5, the radius of the integrating element R_E = 0.0016 mm, the sampling step d = 0.0038 mm

intensity values. For the sampling steps much greater than the sizes of the integrating element and the radii R_φ^{I} of the first minimum of the spread function (which is the case in the example given above) the

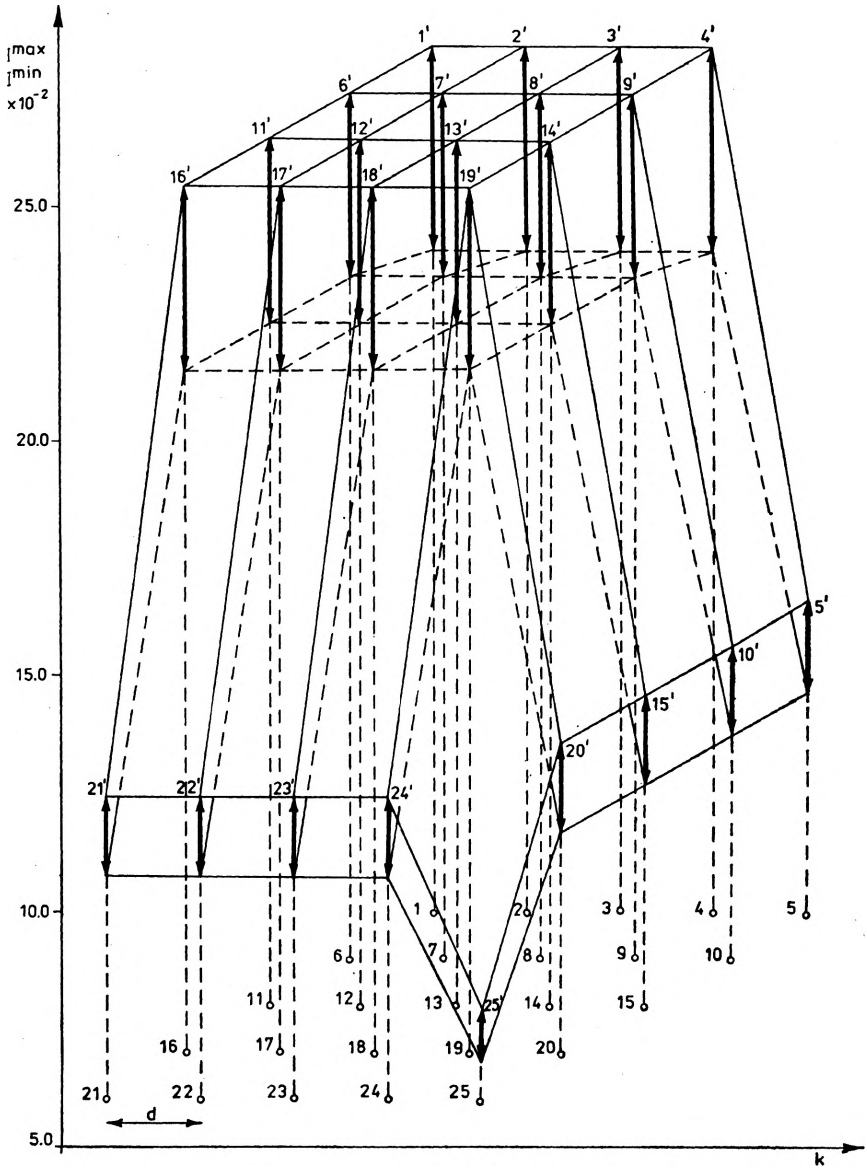

Fig. 8. The upper and lower bound reconstruction of the image intensity distribution. The f-number of the imaging system 4.5, the radius of the integrating element R_E = 0.0016 mm, the sampling step d = 0.0064 mm

lower bound reconstruction process is based only on small energy contributions from the boundary region of the spread function. These contributions are very small in comparison with those coming from the region I of the spread function (and having the decisive influence on the upper bound reconstruction process) and additionally suffer from a greater numerical error. That is why the solution of the reconstruction equation

Table 5

The influence of the number of imaged points on the reconstruction error ΔI; R_E — radius of the integrating element, k — sequential number of sampling points, d — sampling step, s^{upper}, s^{lower} — number of the image points taking immediate part in the intensity reconstruction at the k-th sampling point

k	R_E	d = 0.0032 mm			d = 0.0064 mm		
		s^{upper}	s^{lower}	ΔI $\times 10^{-2}$	s^{upper}	s^{lower}	$I = 10^{-2}$
1	0.0032 mm	8	13	4.06	3	4	5.62
2		11	16	0.98	4	4	5.56
3		13	16	2.06	4	4	5.56
4		11	13	3.19	4	4	5.60
5		8	9	0.40	3	2	2.78
7		15	20	1.60	5	4	5.50
13		21	21	1.03	5	4	5.50
19		15	13	2.47	5	4	5.56
25		8	6	0.85	3	1	1.66
1	0.0016 mm	8	9	4.92			
2		11	12	4.34			
3		13	12	4.45			
4		11	9	4.66			
5		8	6	2.22			
7		15	16	3.88			
13		21	16	4.05			
19		15	9	4.99			
25		8	4	1.32			

(7) obtained for the same postulated results of sampling are inconsistent with physical intuition. The intensity inversion caused by the decrease of numerical accuracy may be observed for great sampling steps and small integrating elements ($R_E \ll R_\varphi^I$) both for the single points and the whole reconstructed region. However, in the case of aberration-free systems the inversion is always a signal that the accuracy of numerical calculations is insufficient.

The influence of the imaging system f-number and the sizes of the integrating element on the image intensity distribution

The change of the imaging system f-number may cause the respective changes of the conventional domain of the intensity spread function.

The effects observed by increasing the f-number of the imaging system should be similar to those occurring for increased sampling steps. In fact, the graphs of the lower and upper image intensities (fig. 10) as well as the

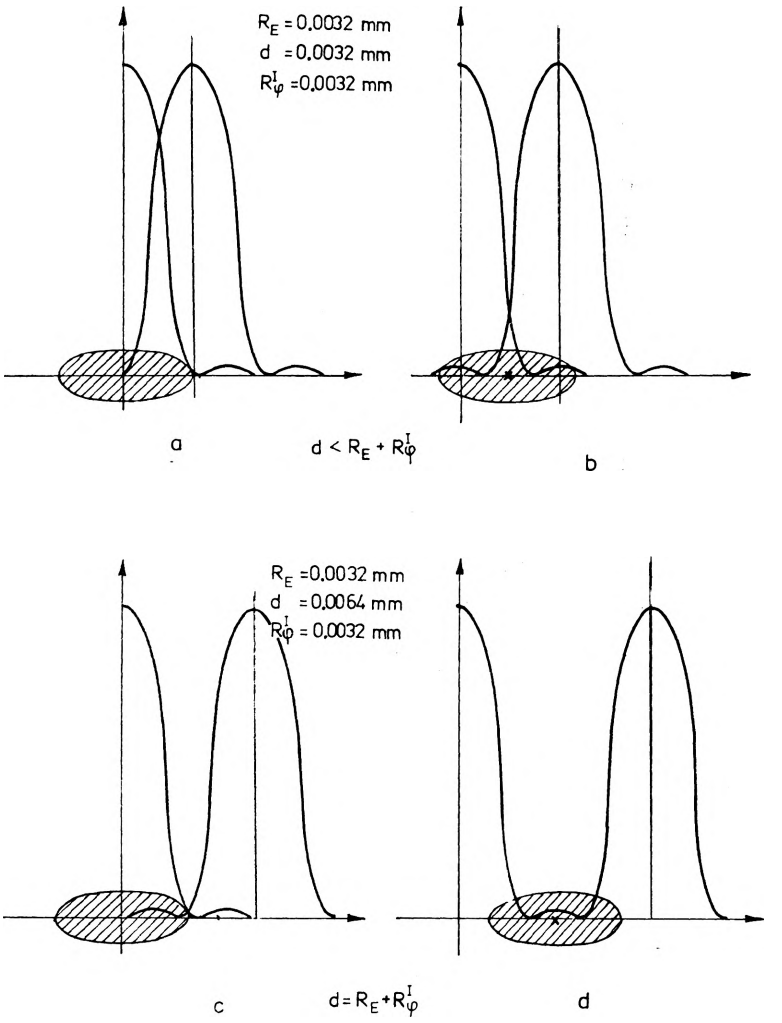

Fig. 9. Changes in the mutual position of the spread function and the integrating element (detector) vs. the sampling step
a – upper reconstruction, b – lower reconstruction, c – upper reconstruction, d – lower reconstruction

changes in the reconstruction error caused by an increase of the f-number confirm this supposition.

The changes in the extreme recovered intensity distributions caused by an increase of the integrating element sizes may be interpreted in a similar way (fig. 11).

The course of these curves may be also justified in another way by comparing the average reconstructed values of intensity with the corresponding average intensities calculated as

$$\langle y(p_k, q_k)\rangle = \frac{y(p_k, q_k)}{S_E}\, 10^{-6}, \tag{14}$$

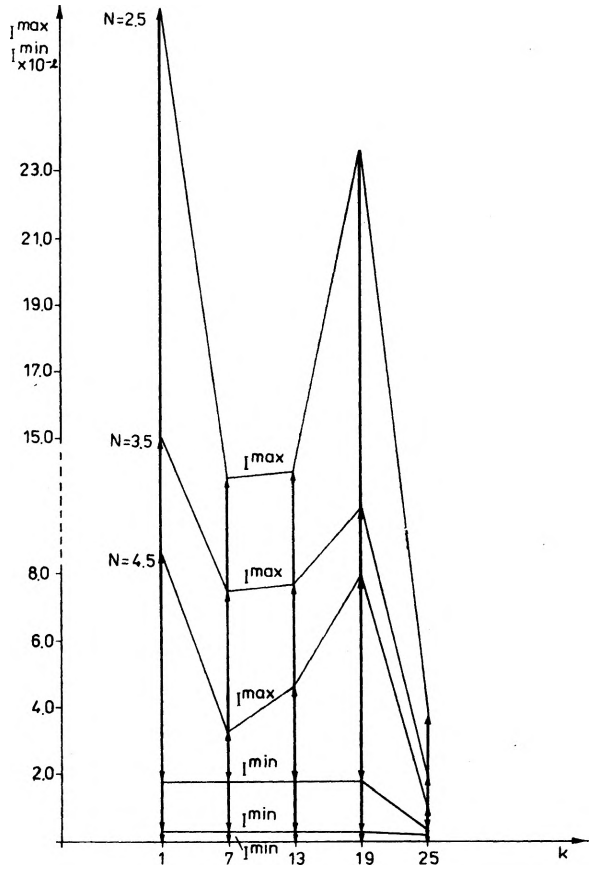

Fig. 10. The influence of the change in the f-number of the imaging system on the upper and lower bound reconstruction of the image intensity distribution (for k points from the reconstructed region diagonal, $R_E = 0.0032$, $d = 0.0032$)

where $y(p_k, q_k)$ is the result of sampling in the k-th sampling point normed for numerical reasons by the factor 10^{-6}, and S_E denotes the area of the integrating element. From the eq. (14) it may be seen that for fixed results of sampling the increase of the integrating element should cause the respective decrement in the average reconstructed intensity distribution, which may be also observed in fig. 11.

The numerical results in table 6 indicate very good agreement of the average intensity values calculated from (14) with those of the average reconstructed intensities. These agreement becomes poorer for greater distances between two successive sampling points. In the case of inversion of extreme intensity distributions caused by diminishing estimation accuracy of the reconstruction matrix elements the average reconstructed intensity may be several times greater than that calculated from (14).

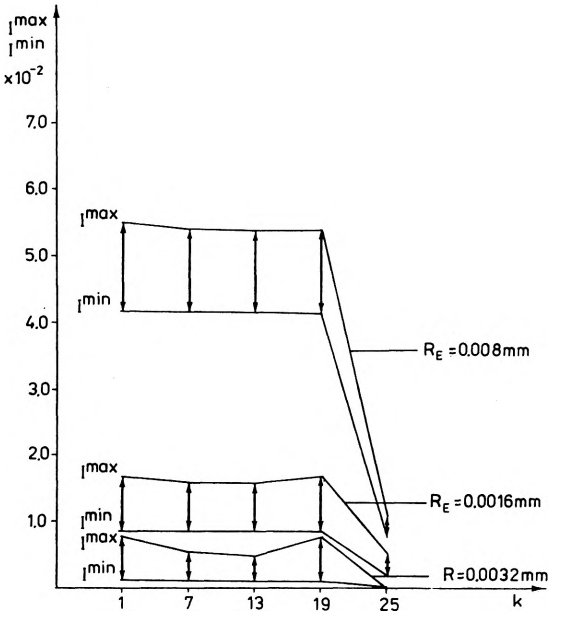

Fig. 11. The influence of the changes in the size of the integrating element radius on the upper and lower bound reconstruction of the image intensity distribution (for selected image points from the diagonal of the reconstructed region). The f-number 4.5, $d = 0.0032$ mm

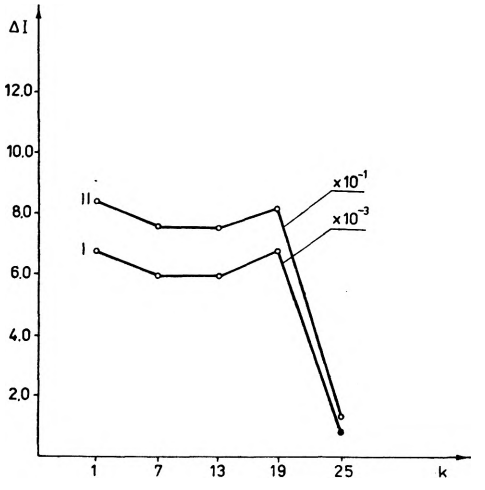

Fig. 12. A comparison of the reconstruction errors for unreduced and reduced measuring systems (for the points lying on the diagonal of the reconstructed region)

Table 6

A comparison of the average postulated intensity distribution with the average reconstructed one

R_E = 0.0016 mm					f-number 4.5					d = 0.0032 mm
Average postulated intensity distribution					Average reconstructed intensity distribution					
0.124	0.124	0.124	0.124	0.062	0.128	0.125	0.125	0.125	0.063	
0.124	0.124	0.124	0.124	0.062	0.125	0.123	0.123	0.124	0.062	
0.124	0.124	0.124	0.124	0.062	0.125	0.125	0.124	0.124	0.062	
0.124	0.124	0.124	0.124	0.062	0.125	0.124	0.124	0.125	0.062	
0.062	0.062	0.062	0.062	0.037	0.063	0.062	0.062	0.062	0.038	

Effect of the measuring system reduction on the reconstruction process

The intensity measurement in the image plane may be carried out in two ways: either with the help of the measuring system (optical part plus the integrating element), or by locating the integrating element immediately in the image plane at the respective sampling point. In table 7 and in fig. 12 the reconstructed errors for both these cases are compared under assumption that the f-numbers of both the systems are the same and the radius

Table 7

A comparison of the reconstructed intensity distribution obtained with the help of unreduced and reduced measuring system. The f-numbers of the imaging and measuring systems are assumed to be the same

Unreduced measuring system					Reduced measuring system				
Upper bound image intensity distribution $I^{\max} \times 10^{-1}$					Lower bound image intensity distribution $I^{\max} \times 10^{-2}$				
1.739	1.672	1.676	1.710	0.837	1.604	1.608	1.608	1.606	0.804
1.674	1.596	1.599	1.638	0.798	1.608	1.612	1.612	1.610	0.806
1.676	1.596	1.601	1.640	0.799	1.608	1.611	1.612	1.610	0.806
1.710	1.637	1.640	1.676	0.821	1.606	1.610	1.610	1.608	0.805
0.837	1.798	0.799	0.821	0.306	0.804	0.806	0.806	0.805	0.323
Lower bound image intensity distribution $I^{\min} \times 10^{-2}$					Lower bound image intensity distribution $I^{\min} \times 10^{-3}$				
5.548	7.384	7.384	5.548	3.511	2.597	3.433	3.433	2.597	1.633
7.348	9.183	9.183	7.384	4.618	3.433	4.268	4.268	3.433	2.134
7.384	9.183	9.183	7.384	4.618	3.433	4.268	4.268	3.433	2.134
5.548	7.384	7.384	5.548	3.511	2.597	3.433	3.433	2.597	1.633
3.511	4.618	4.618	3.511	2.611	1.633	2.134	2.134	1.633	1.188

of the integrating element is four time less than the sampling step. The magnification of the system II is assumed to be equal to unity. As a result of the image intensity reconstruction from the sampling data obtained with the reduced system (integrating element) the recovered intensity distributions and the reconstruction errors are less than those obtained by using the nonreduced measuring system, but the general character of the changes in both cases remains the same. This results is only an example, which should not be generalized without due criticism.

Conclusions

In summing up the examples discussed it may be stated that:

a. The direct recovery method is very sensitive to the changes in intensity distribution within the aberrational spot.

b. There exist some limitations in the selection of sampling steps caused both by diminishing accuracy of numerical calculation for large sampling steps and by some objective properties of the imaging system.

The direct recovery procedure for the sampling steps not less than the respective Rayleigh distances may be succesfully performed. By choosing the integrating elements to be small enough it is possible to make the sampling steps even smaller than the Rayleigh distance with the recovery procedure still working. For instance, for the imaging system of the f-number 4.5 by reducing the radius of the integrating element to its half-value it is possible to diminish the sampling steps to the value $d = 2 \cdot 10^{-4}$ mm. For the further reduced sampling steps there appear negative roots of the reconstruction eq. (7) which is inconsistent with their physical sense and may be considered as a signal that the applicability limits of the recovery procedure have been overcome. This limitation of the least admissible sampling step is comprehensible. It may not be less than the distance corresponding to the cut-off frequency of the system. For instance, for the aberration-free system of the f-number 4.5 and the wavelength $\lambda = 0.0058$ mm the cut-off frequency is $f_{co} = 382$ mm^{-1} and the corresponding sampling steps is $d = 0.0026$ mm.

There exists also some limitation of the maximal sampling step. This follows from the fact that for numerical reasons the domain of the spread function is reduced to the second (or third) minimum, i.e. the sampling step must fulfil the condition

$$d < 2R_E + R^{\mathrm{II}\min},$$

where $R^{\mathrm{II}\min}$ is the radius of the spread function domain. In reality, the reduction in the numerical calculation accuracy of the matrix elements for the border values of the spread function makes this distance still lower.

By changing the sizes of the integrating element it is possible to shift the limiting value of the sampling step. For the small integrating elements the achieved sampling step may be slightly less than the Rayleigh distance but then the upper admissible value of the sampling step is lowered (to the distance close to the second maximum of the spread function). For the large integrating elements small sampling steps may not be realized*. For instance, for the imaging system of f-number 4.5, and the integrating element radius $R_E = 0.004$ mm the last sampling step is $d = 0.0045$ mm but then the maximal admissible distence between the sampling points is much greater.

References

[1] Barnes C. W., J. Opt. Soc. Am. **56** (1966), 575.
[2] Frieden B. R., J. Opt. Soc. Am. **57** (1967), 1013.
[3] Wilk I., Pr. nauk. Inst. Fiz. PWr., Studia i Materiały Nr 2, Wrocław 1969, p. 9.
[4] Wilk I., Pr. nauk. Inst. Fiz. PWr., Nr 4, Wrocław 1970, p. 3.
[5] Wilk I., Optica Applicata **II** (1971), 37.
[6] Nowak R., Maliszewski E., Wilk I., Optica Applicata **IV** (1974), 37.
[7] Wilk I., Zeszyty Naukowe Politechniki Wrocławskiej, Fizyka **XV**, Nr 214.

Received, November, 21, 1979

Численная реконструкция распределения интенсивности в некогерентном изображении. I. Дифракционные системы

Обсуждаются свойства метода непосредственной реконструкции распределения интенсивности в изображении. Этот метод даёт возможность воспроизвести предмет наблюдения на основе его измерительных данных. Исследовали с помощью численных данных влияние многих факторов, таких как число точек испытания образца, шаг испытания, размеры интегрирующего элемента на обсуждаемый способ реконструкции. Рассмотрен случай как одномерный, так и двумерный. Показано, что метод непосредственной реконструкции очень чувствителен даже на небольшие изменения распределения интенсивности в аберрационном пятне.

---

* The remarks are valid for the numerical reconstruction, especially if applied to the numerically simulated experiments considered in this paper. They have to be reconsidered if applying the recovery procedure to the sampling of the real images.